1-31-2007

Characteristics of an evaporating thin film in a microchannel

Hao Wang

S V. Garimella
Purdue Univ, sureshg@purdue.edu

Jayathy Y. Murthy

Available online at www.sciencedirect.com
ScienceDirect
International Journal of Heat and Mass Transfer 50 (2007) 3933–3942
International Journal of HEAT and MASS TRANSFER
www.elsevier.com/locate/ijhmt

Characteristics of an evaporating thin film in a microchannel

Hao Wang, Suresh V. Garimella *, Jayathi Y. Murthy

Cooling Technologies Research Center, School of Mechanical Engineering, Purdue University, West Lafayette, IN 47907-2088, USA

Received 14 September 2006; received in revised form 31 January 2007
Available online 11 April 2007

Abstract

An evaporating meniscus in a microchannel is investigated through an augmented Young–Laplace model and the kinetic theory-based expression for mass transport across a liquid–vapor interface. The complete expression for mass transport is employed without any approximations and boundary conditions for the film profile are developed. The thin film and the intrinsic-meniscus regions are distinguished based on the disjoining pressure variation along the meniscus. While heat transfer in the thin-film region is found to be relatively insensitive to channels larger than a few micrometers in radius, that in the intrinsic meniscus is quite sensitive to channel size. The role of evaporation suppression due to capillary pressure in both regions is discussed. Compared to the relatively small contribution to overall heat transfer from the thin-film region, the micro-region (defined here as extending from the non-evaporating region to a location where the film is 1 μm thick) is found to account for more than 50% of the total heat transfer.

Keywords: Meniscus; Thin-film; Triple line; Microchannel; Evaporation; Liquid cooling

1. Introduction

When a liquid wets a solid wall, the extended meniscus can typically be divided into three regions as illustrated in Fig. 1: an adsorbed or non-evaporating region where liquid is adsorbed on the wall; a thin-film or transition region where effects of long-range molecular forces (disjoining pressure) are felt; and an intrinsic meniscus region where capillary forces dominate. Of these, the thin-film region is characterized by high heat transfer rates because of the very low thermal resistance across the liquid film. Porous or grooved surfaces can help to create thin films for enhanced operation of heat transport devices such as heat pipes and capillary pumped loops.

Deryagin et al. [1,2] demonstrated liquid pressure reduction in the thin-film region due to disjoining pressure. Potash and Wayner [3] concluded that the variation of disjoining pressure and capillary pressure along the meniscus provides the necessary pressure gradient for liquid supply into the thin-film region. Wayner et al. [4] discussed the effects of disjoining pressure on liquid supply as well as its role in suppressing evaporation. An augmented Young–Laplace equation was obtained for force balance on the thin film by introducing a disjoining pressure such that $P_v = P_l + P_c + P_d$. Schonberg et al. [5] investigated the thin film by ignoring P_c. Hallinan et al. [6] and DasGupta et al. [7] developed a fourth-order ordinary differential equation for solving the augmented Young–Laplace equation and obtained the thickness profile of the extended meniscus. The influence of superheat on the thin-film profile was discussed. Park et al. [8] proposed a mathematical model which included the vapor region and a slip boundary condition. It was concluded that the pressure gradient in the vapor region significantly affected the thin-film profile. Wee [9] discussed the effects of liquid polarity, slip boundary and thermocapillary effects on the thin-film profile. The polarity effect was found to elongate the transition region while suppressing evaporation. Recently, binary liquids [10] have been found to induce a distillation-driven capillary stress to counteract the thermocapillary stress, leading to an elongation in thin-film length. Atomistic simulations by Freund [11] showed that the thermal resistance at the

* Corresponding author. Tel.: +1 765 494 5621.
E-mail address: sureshg@purdue.edu (S.V. Garimella).

0017-9310/$ - see front matter © 2007 Elsevier Ltd. All rights reserved.
doi:10.1016/j.ijheatmasstransfer.2007.01.052

Nomenclature

A	dispersion constant (J)
H	height of channel (m)
h_{fg}	latent heat of evaporation (J/kg)
k_l	liquid conductivity (W/mK)
m'	mass flow rate (kg/ms)
m''	interface net mass flux (kg/m^{2}s)
$\overline{M}$	molecular weight (kg/mol)
$\overline{R}$	universal gas constant (J/mol K)
P_d	disjoining pressure (N/m^2)
P_l	liquid pressure (N/m^2)
ΔP_l	change of liquid pressure (N/m^2)
P_{sat}	saturation pressure (N/m^2)
P_v	vapor pressure (N/m^2)
P_{v_equ}	equilibrium pressure (N/m^2)
q	integrated heat transfer rate (W/m)
R	meniscus radius (m)
R^*	asymptotic intrinsic meniscus radius (m)
T	temperature (K)
u	velocity along x-axis (m/s)
V	molar volume (m^3/mol)
x	x-coordinate (m)
y	y-coordinate (m)

Greek symbols

δ	liquid layer thickness (m)
δ_0	non-evaporating layer thickness (m)
v	kinematic viscosity (m^2/s)
μ	dynamic viscosity (Ns/m^2)
ρ_l	liquid density (kg/m^3)
ρ_v	vapor density (kg/m^3)
σ	surface tension coefficient (N/m)
$\hat{\sigma}$	accommodation coefficient

Subscripts

c	condensation
e	evaporation
l	liquid
lv	liquid–vapor interface
sat	saturated
sum	sum
t	thin-film region
v	vapor
ref	reference state

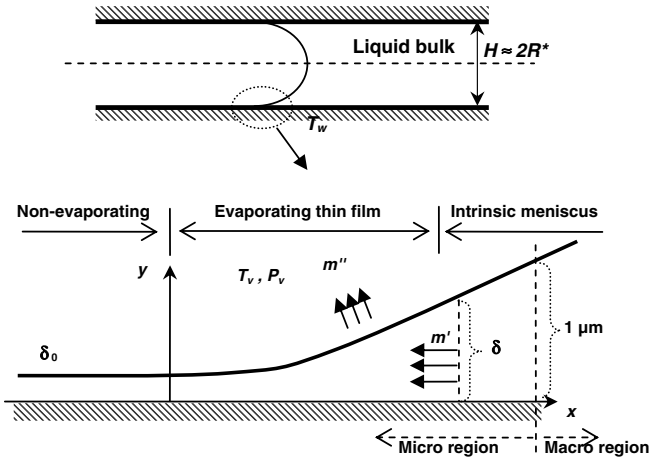

Fig. 1. Schematic diagram and coordinate system for an evaporating thin film in a channel.

solid–liquid interface is significant in very thin films. A Kapitza resistance was employed to obtain the solid–liquid interface temperature.

The menisci in more complex geometries have also been studied. Stephan and Busse [12] calculated the heat and mass transfer in the micro-region and then combined the solution with the macroscopic meniscus within open grooves. Xu and Carey [13] conducted a combined analytical and experimental investigation on the liquid flow in V grooves and emphasized the importance of disjoining pressure on the overall heat transfer. Ma and Peterson [14] proposed a mathematical model for the evaporation heat transfer coefficient and temperature variation along the axial direction of a groove, which led to a better understanding of the axial heat transfer coefficient and temperature distribution on grooved surfaces. Morris [15] suggested a universal relationship between heat flow, contact angle, interface curvature, superheat and material properties, which can be extended to different geometries. Recently, thin-film evaporation in a microchannel was studied [16]. The thin-film was maintained throughout at a temperature below the saturation temperature corresponding to the imposed pressure, and the gas domain was assumed to consist of a mixture of air and vapor. The vapor diffusion in the gas domain was calculated to obtain evaporation flux, and heat transfer results in the form of a local Nusselt number were reported.

In the present work, an evaporating meniscus in a channel is investigated. The meniscus is superheated, and vapor space is assumed to consist of pure saturated vapor. The present model complements previous studies [3–16] in three ways. First, heat transfer in the thin-film and micro-regions is quantitatively compared and the relative contributions of the two regions to the overall heat transfer delineated. Second, the kinetic theory-based expression for mass transport across a liquid–vapor interface [17] is used instead of a simplified version often adopted in prior studies (which assume $T_{lv} \approx T_{sat}$); the simplified expression is shown in this work to underpredict the total heat transfer at high superheats. Third, the influence of capillary suppression and channel size on heat transfer from the thin-film region is discussed in detail.

2. Theoretical model

2.1. Thin-film profile

The equations governing the thin-film profile have been extensively discussed in the literature [3–9] and are briefly reviewed here. The pressure difference between vapor and liquid at the liquid–vapor interface is due both to the capillary and disjoining pressures, and is expressed using the augmented Young–Laplace equation [4]:

$$P_v = P_l + P_c + P_d \tag{1}$$

The disjoining pressure for a non-polar liquid is expressed as [4,18]

$$P_d = A/\delta^3 \tag{2}$$

where A is the dispersion constant and δ the film thickness. The capillary pressure is the product of interfacial curvature K and surface tension coefficient σ

$$P_c = \sigma K, \quad K = \delta''(1+\delta'^2)^{-1.5} \tag{3}$$

where δ' and δ'' are, respectively, the first and second derivatives of thickness with respect to length x. The model is often simplified in the literature by assuming a value of zero for δ' [6–9]. This term is retained in the present work to better model the beginning of the intrinsic meniscus where the slope may not be negligible. The problem under consideration is illustrated in Fig. 1.

Combining Eqs. (1)–(3) and differentiating with respect to x, the following third-order differential equation is obtained for the thin-film profile $\delta(x)$:

$$\delta''' - \frac{3\delta'\delta''^2}{1+\delta'^2} + \frac{1}{\sigma}\left(\frac{dP_l}{dx} - \frac{3A}{\delta^4}\delta'\right)(1+\delta'^2)^{1.5} = 0 \tag{4}$$

assuming uniform P_v along the meniscus. In view of the very low Reynolds number and the large length-to-height ratio of the thin film, lubrication theory is employed to obtain the pressure gradient in Eq. (4). A no-slip boundary condition at the wall and a no-shear boundary condition at the liquid–vapor interface are imposed. Under these assumptions, the liquid pressure gradient dp_l/dx may be related to the mass flow rate $m\prime(x)$. At steady state, the mass flow rate $m\prime(x)$ at a position x is equal to the integral of the net evaporative mass flux from the beginning of the film to the local position. The liquid pressure gradient may then be obtained as

$$\frac{dP_l}{dx} = \frac{3v}{\delta^3}\int_{-\infty}^{x} m''\,dx \tag{5}$$

Substituting the pressure gradient into Eq. (4) and further differentiating with respect to x, a fourth-order ordinary differential equation is obtained for the thin-film profile:

$$\frac{d}{dx}\left(\left[\frac{\sigma\delta'''}{(1+\delta'^2)^{1.5}} - \frac{3\sigma\delta'\delta''^2}{(1+\delta'^2)^{2.5}} - \frac{3A\delta'}{\delta^4}\right]\frac{\delta^3}{3v}\right) = -m'' \tag{6}$$

The local evaporation mass flux m'' is determined from the interfacial mass transport as discussed below.

2.2. Interfacial mass transport

As reviewed in [19], Schrage [17] proposed a theory for evaporation at an interface, in which the net mass flux across the interface $m\prime\prime$ is the difference between the fluxes of pure condensation m''_c and pure evaporation m''_e, i.e., $m'' = m''_e - m''_c$. Assuming the evaporation coefficient and the condensation coefficient to be equal to each other for simplicity as suggested in the reviews in [19,28], the net mass flux may finally be written in the form that is employed in the present thin-film model:

$$m'' = \frac{2\hat{\sigma}}{2-\hat{\sigma}}\left(\frac{\overline{M}}{2\pi\overline{R}}\right)^{1/2}\left(\frac{P_{v\_equ}(T_{lv})}{T_{lv}^{1/2}} - \frac{P_v}{T_v^{1/2}}\right) \tag{7}$$

The equilibrium vapor pressure P_{v_equ} is the pressure at which the vapor is in equilibrium with the liquid. For a flat interface on a bulk liquid (no capillary or disjoining pressure), P_{v_equ} is equal to the saturation pressure P_{sat} at T_{lv} [20]. In a thin film, however, the disjoining pressure and capillary pressure affect the equilibrium state and P_{v_equ} is not equal to P_{sat}, but is in fact smaller [21]:

$$P_{v\_equ}(T_{lv}) = P_{sat}(T_{lv})\exp\left[\frac{P_{v\_equ}(T_{lv}) - P_{sat}(T_{lv}) - (P_d + P_c)}{\rho_l T_{lv}\overline{R}/\overline{M}}\right] \tag{8a}$$

where

$$P_{sat}(T_{lv}) = P_{sat\_ref}(T_{sat\_ref})\exp\left[\frac{\overline{M}h_{fg}}{\overline{R}}\left(\frac{1}{T_{sat\_ref}} - \frac{1}{T_{lv}}\right)\right] \tag{8b}$$

It is seen that the role of disjoining and capillary pressures is to reduce $P_{v\_equ}(T_{lv})$, and thus, to suppress evaporation. There is much debate about the value of the accommodation coefficient [22,28], especially for polar liquids such as water and methanol. In experiments, non-polar liquids commonly have yielded higher accommodation coefficients than polar liquids. Non-polar liquids including carbon tetrachloride, benzene, and hexadecane have been experimentally found to have an accommodation coefficient of unity [22,28]. In the present work, since octane is a non-polar liquid, we assume its accommodation coefficient to be unity. More accurate values would require more detailed experiments.

In the development thus far, T_{lv} is unknown. However, it is noted that the evaporation heat flux on the interface is equal to the conduction heat flux through the thin film:

$$m''h_{fg} = \frac{k_l(T_w - T_{lv})}{\delta} \tag{9}$$

By solving Eqs. (7)–(9) together, $T_{lv}, P_{sat}, P_{v\_equ}$, and m'' are obtained; of these, the calculated m'' is used to compute the thin-film profile via Eq. (6).

In much of the published literature [4–6,9,10] m'' is calculated using the evaporation model proposed by Wayner et al. [4]:

$$m'' = a(T_{lv} - T_v) - b(p_d + p_c) \tag{10a}$$

where $a = C\left(\frac{\overline{M}}{2\pi\overline{R}T_{lv}}\right)^{1/2}\frac{P_v\overline{M}h_{fg}}{\overline{R}T_vT_{lv}}$,

$$b = C\left(\frac{\overline{M}}{2\pi\overline{R}T_{lv}}\right)^{1/2}\frac{V_lP_v}{RT_{lv}} \tag{10b}$$

The second term on the right-hand side of Eq. (10a) represents the suppression of the evaporation rate by disjoining and capillary pressures. It was simplified from Schrage's original expression, Eq. (7), by using an extended Clapeyron equation [4] and the approximations $T_{lv} \approx T_v$ and $P_{v\_equ} \approx P_v$. A comparison of the evaporation heat transfer coefficient calculated from the original expression in Eq. (7) as $h_{lv} = m''h_{fg}/(T_{lv} - T_v)$ with that calculated from Wayner's equation (10) is shown in Fig. 2 for different superheats. It is seen that the two equations yield nearly identical results for superheats under 5 K, but that Eq. (10) significantly underestimates h_{lv} for large superheats. Superheats considered in the literature [4–6,9,10] have been generally lower than 1 K, which has allowed use of the simplified form in Eq. (10). However, under high heat fluxes, such as in Schonberg et al. [23] who encountered a superheat of 5.2 K, the simplified form would lead to an underestimation of h_{lv}. High superheats are also expected in the meniscus at the bottom of a bubble during boiling. In the present work, Schrage's original expression is employed to allow for the study of higher superheats. A detailed analysis of the impact of the use of Eq. (10) versus Eq. (7) in thin-film calculation is presented in Section 3.3.

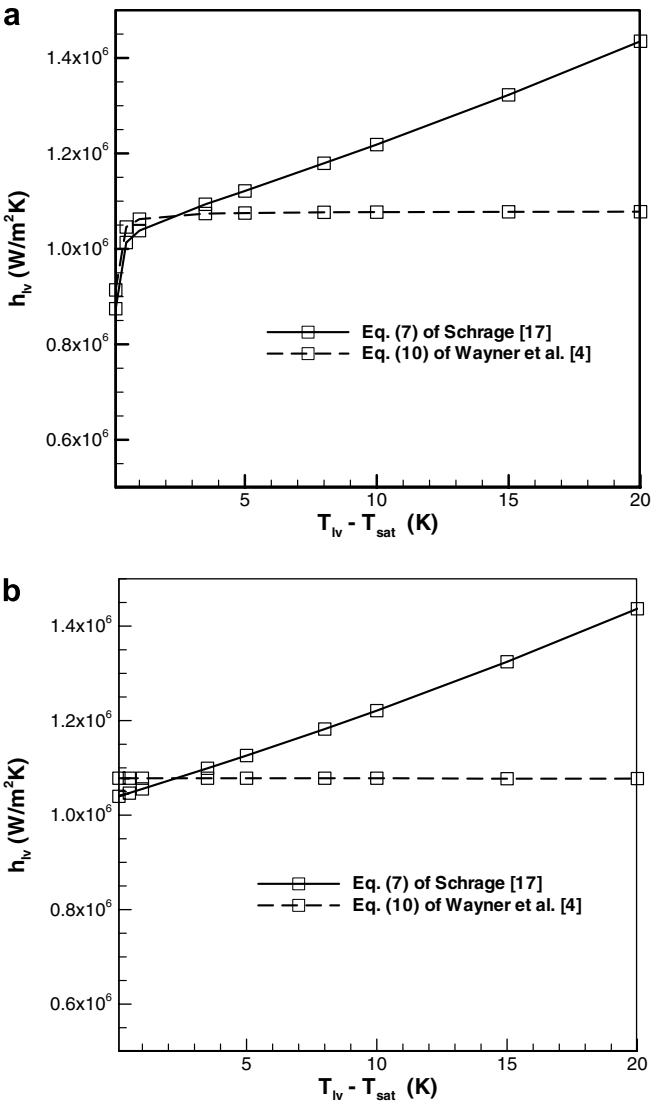

Fig. 2. Comparison of mass fluxes obtained using Eq. (7) from Schrage [17] and Eq. (10) from Wayner et al. [4]. The calculations are performed for octane with properties as in Table 1. A value of (a) 104 Pa, and (b) 0 Pa is assumed for suppression pressure ($P_d + P_c$).

2.3. Solution method and boundary conditions

The particular system considered is the evaporation of a film of octane on a silicon substrate. The vapor domain is assumed to be saturated at T_v and P_v. The relevant properties are listed in Table 1. The dispersion constant A is assumed to be 3.18×10^{-21} J based on the data in [24], which considered octane on silicon with air at room temperature. The accommodation coefficient $\hat{\sigma}$ for the evaporation calculation is assumed to be unity for octane, a non-polar liquid, as discussed earlier. These values, $A = 3.18 \times 10^{-21}$ J and $\hat{\sigma} = 1$, were also used in [5].

Eq. (6) is a fourth-order, non-linear ODE and can be treated as an initial-value problem by specifying the conditions at the beginning of the thin-film region, $x = 0$, where the non-evaporating film ends and the evaporating thin film starts, as shown in Fig. 1. Four initial conditions are needed, i.e., $\delta(x = 0)$, $\delta'(0)$, $\delta''(0)$, and $\delta'''(0)$. The method proposed by Dormand and Prince [25] is employed to solve this equation. The initial thickness $\delta(0)$ should be equal to the non-evaporating thickness δ_0, which is obtained by setting the net mass flux to zero in Eq. (7). Setting $m'' = 0$ and $T_{lv} = T_w$ (interface temperature in the non-evaporating region is approximated to be the wall temperature [4,5]) in Eq. (7) gives P_{v_equ}; substituting P_{v_equ} into Eq. (8), the sum of the disjoining and capillary pressures needed to completely suppress evaporation is obtained as

Table 1
Properties of evaporating liquid [5] and operating conditions

Liquid	Octane
A (J)	3.18×10^{-21}
P_v (Pa)	1.5828×10^4
ρ_l (kg/m^3)	661.2
k_l (W/mK)	0.11
h_{fg} (kJ/kg)	339.8
T_w (K)	344
T_v (K)	343
$\hat{\sigma}$	1

$$P_{d0} + P_{c0} = -\rho_l T_w \frac{\overline{R}}{\overline{M}} \ln\left(\sqrt{\frac{T_w}{T_v}} \frac{P_v}{P_{sat}(T_w)}\right) + P_v\sqrt{\frac{T_w}{T_v}} - P_{sat}(T_w) \quad (11)$$

Assuming that the curvature of the non-evaporating region is zero, $P_{c0} = 0$. Then P_{d0} is obtained, from which the thickness of the non-evaporating region δ_0 can be computed. For octane with 1 K superheat, values of $P_{d0} = 6.3 \times 10^5$ Pa and $\delta_0 = 1.71$ nm are obtained.

However, it is found that if δ_0 is used as the thickness at $x = 0$, the evaporation mass flux is zero along the entire (extended) meniscus for the following two reasons. (a) At $x = 0$, $\int_{-\infty}^{x} m'' \, dx = 0$, so that $(dP_l/dx) = 0$ according to Eq. (5). Furthermore, $d(P_c + P_d)/dx = 0$. Since the suppression of evaporation is determined by $P_c + P_d$, this latter condition implies that this suppression effect does not change with film thickness, so that $dm''/dx = 0$. (b) With $m'' = 0$ and $dm''/dx = 0$ at $x = 0$, $m'' = 0$ is found at the next step $x = 0 + dx$, which renders the accumulated mass flux $\int_{-\infty}^{x} m'' \, dx$ to continue to be zero along x. Continuing this analysis, each successive step also has zero evaporative mass flux, so that the entire thin film would have no evaporation. Thus, a value slightly larger than δ_0 is chosen as the condition at $x = 0$. Since evaporation near the beginning of the thin-film region is negligible, this perturbation has an insignificant influence on the overall thin-film heat transfer. This is seen in the plot of cumulative heat transfer $q(x)$ up to location x and capillary pressure P_c for two different choices of $\delta(0)$, 1.8 and 3.4 nm, in Fig. 3. In the calculations presented in this paper, $\delta(0) = 3.4$ nm is used.

In terms of the other three conditions at $x = 0$, the initial slope for a completely wetting film is close to zero; in the present work, $\delta'(0) = 1 \times 10^{-11}$ is used. Further reducing the value to zero does not significantly change the resulting film profile. Since $\delta''(0)$ cannot be specified directly, a far-field boundary condition is used as in [6,23]. In [23], the far-field condition is set by assuming that the film slope approaches a constant value (i.e., the meniscus radius R approaches infinity). For a meniscus in a channel, however, R should approach the constant radius R^* in the intrinsic meniscus, which is approximately half of the channel height H when the liquid is completely wetting [26,27]. The variation of meniscus radius with respect to x is discussed further in Section 3. Iterative calculations are employed to obtain $\delta''(0)$ for a specified R^* by changing $\delta''(0)$ until the desired value of R^* is obtained. The imposition of the far-field curvature R^* is found to be critical. It is found that small changes in $\delta(0)$ or $\delta'(0)$ make negligible difference to the thin-film profile and heat transfer characteristics as long as R^* is the same, as in the example shown in Fig. 3. The fourth condition, $\delta'''(0)$, is obtained from Eq. (4) in terms of $\delta(0), \delta'(0)$ and $\delta''(0)$, together with $\int_{-\infty}^{0} m'' \, dx = 0$. This fourth condition has a very weak influence on the thin-film profile obtained.

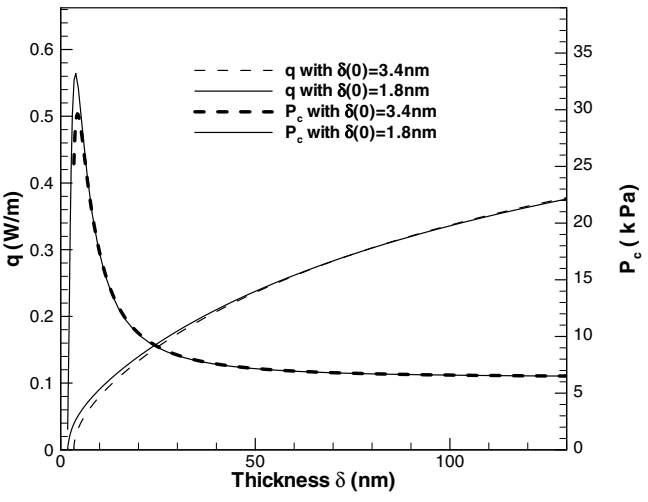

Fig. 3. Influence of initial thin-film thickness $\delta(0)$ on the cumulative heat transfer from the thin-film region as well as on the capillary pressure (intrinsic meniscus radius $R^* = 2500$ nm).

3. Results and discussion

Characteristics of the thin-film region are presented in this section, based on the model developed above, which employs the evaporation model of Schrage [17]. The variations of different pressure components along the meniscus are analyzed to delineate their effect on evaporation in the thin-film region. The effects on evaporation of suppression due to capillary pressure, wall superheat and channel size are discussed.

3.1. Thin-film characteristics

The variation of disjoining pressure (P_d), capillary pressure (P_c), and liquid pressure change ($\Delta P_l = P_l - P_l(x = 0)$) along the length of the liquid film are plotted in Fig. 4 for two different channel sizes, $R^* = 2500$ nm and $R^* = 200$ nm. The sum of the three components of pressure ($P_{sum} = P_d + P_c + \Delta P_l$) is always a constant along the film length, as expected from the Young–Laplace equation.

The evaporated liquid is replenished by the liquid pressure gradient. For the first 40 nm along the thin-film region, Fig. 4a shows that the increase in liquid pressure is solely supported by the reduction in disjoining pressure. Beyond this length, the capillary pressure also decreases and begins to contribute to the increase in liquid pressure, which is consistent with the observations of [7]. In Fig. 4b, it is seen that the capillary pressure is maintained at a high level and does not drop in the case of the much smaller channel size. The drop in capillary pressure is important for flattening the thickness profile and enhancing liquid pumping. It will be seen later (in Fig. 5) that the greater the drop in capillary pressure, the more flat is the thin film.

The thin-film region is generally understood to be dominated by disjoining pressure while the intrinsic meniscus is dominated by capillary pressure. The locations at which the disjoining pressure drops to 1/100th, 1/1000th,

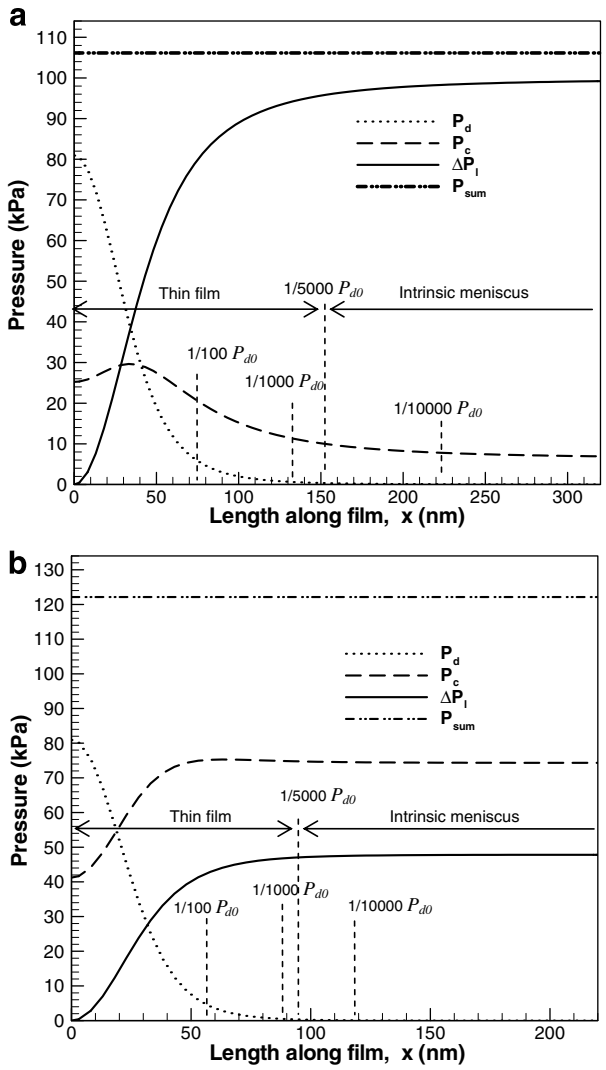

Fig. 4. Variation of the different pressure components along the length of the meniscus (superheat 1 K): (a) $R^* = 2500$ nm and (b) $R^* = 200$ nm.

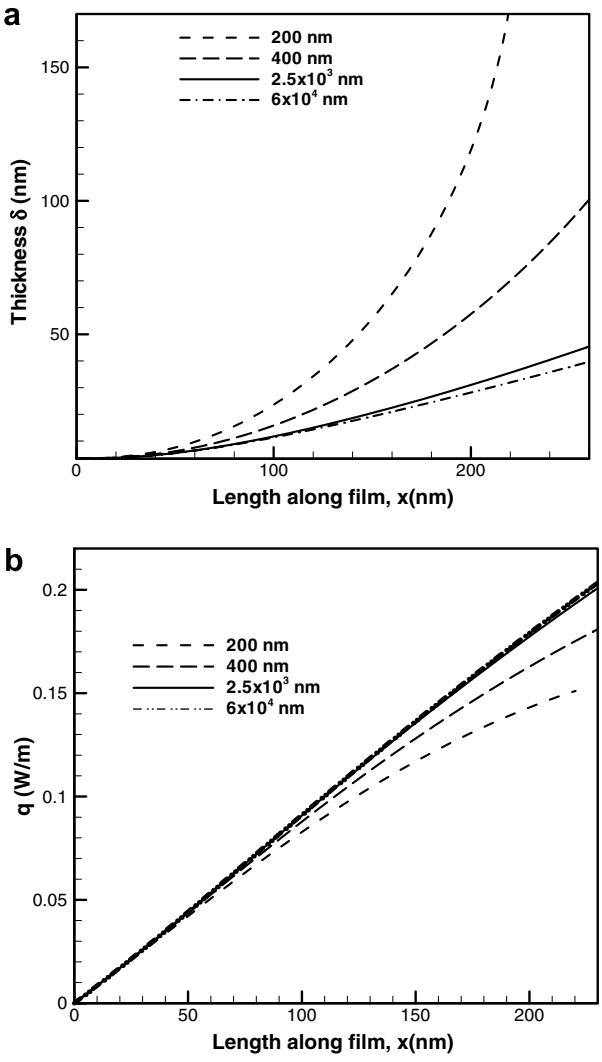

Fig. 5. Thin film with different channel sizes ($R^* = 200$, 400, 2500, and 6.1×10^4 nm): (a) film thickness and (b) cumulative q.

and 1/10,000th of P_{d0} are marked in Fig. 4a and b. It is seen that disjoining pressure ceases to contribute to P_l once it drops to values in the range of 1/1000th of P_{d0}. In the present work, the thin-film region is identified as ending at a location when the disjoining pressure drops to 1/5000th of P_{d0}, beyond which the intrinsic meniscus region starts. For example, in Fig. 4a, the end of the thin-film region is identified as being at $x = 154$ nm, where $P_d = 3.15 \times 10^2$ Pa. At this location, P_d is only 1/300th of P_c and its contribution to the increase in P_l with increasing x is negligible from this location onwards. Similar results are noted from Fig. 4b for a much smaller channel size.

3.2. Intrinsic meniscus radius

In Fig. 4 it is seen that P_c ($=\sigma/R$) approaches a constant value in the intrinsic meniscus, indicating that the film radius approaches the value R^*, which is approximately half of the channel height H when the liquid is completely wetting [6,26,27]. A larger R^* corresponds to a flatter thickness profile so that the thin-film region is larger, as is evident from a comparison of Fig. 4a and b. The importance of R^* is demonstrated by its effect on the thin-film profiles and cumulative heat transfer rate in Fig. 5a and b. A larger R^* corresponds to better thin-film heat transfer, as seen in Fig. 5b.

When the radius R^* exceeds a certain value, however, the thin-film thickness profile $\delta = \delta(x)$ reaches an invariant state: the profiles for $R^* = 2500$ and 6.1×10^4 nm are seen in Fig. 5(a) to be quite similar, and the corresponding heat transfer curves almost overlap each other in Fig. 5(b). As seen in Table 2(a), the thin-film heat transfer q_t does not change much with R^* beyond $R^* > 2500$ nm. The differences due to changes in R^* are most evident in the intrinsic meniscus rather than in the thin-film region.

3.3. Superheat

The meniscus profiles for different levels of superheat from 5 K to 0.01 K are compared in Fig. 6. It is seen that

Table 2
Thin-film region for (a) different channel sizes (superheat 1 K) and (b) different superheats ($R^* = 2500$ nm)

(*a*)						
R^* (nm)	200	2500	6.1×10^4	2.1×10^5		
Thin-film length (nm)	95	154	160	160		
Thickness at the end of thin film (nm)	21	21	21	21		
Thin-film heat transfer q_t (W/m)	0.08	0.139	0.141	0.141		
Percentage contribution to net heat transfer rate	53%	20%	8%	5%		
(*b*)						
Superheat (K)	0.01	0.04	0.1	1	5	20
Thin-film length (nm)	1096	666	585	154	63	28
Thickness at the end of thin film (nm)	99	74	45	21	12	7
Thin-film heat transfer q_t (W/m)	9.5×10^{-5}	1.6×10^{-2}	0.035	0.139	0.32	0.68
Percentage contribution to net heat transfer rate	69%	54%	43%	20%	12%	9%

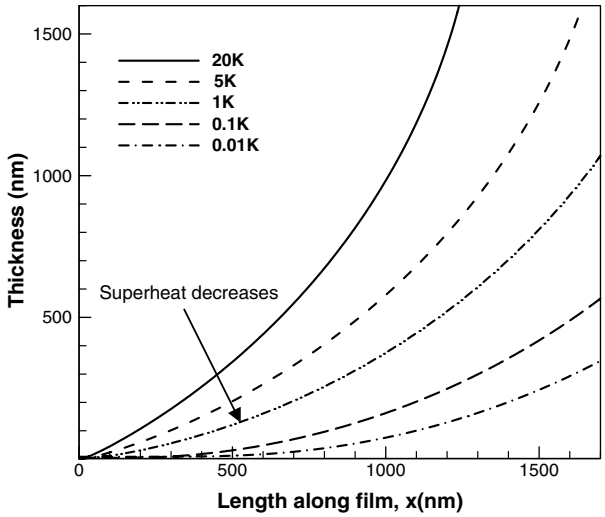

Fig. 6. Effect of superheat on the film thickness profile ($R^* = 2500$ nm).

the apparent contact angle grows with superheat. The decrease in disjoining pressure causes liquid to be pumped into the thin film. When the superheat is increased, evaporation is strengthened and more liquid needs to be pumped into the thin film, decreasing the disjoining pressure faster and finally resulting in a larger apparent contact angle, which is consistent with previous studies [6–9]. Also as seen in Table 2(b), the contribution of the thin film to the overall heat transfer is increased.

In Section 2.2, Eq. (7) [17] and Eq. (10) [4] were compared, and it was found that for larger superheat (>5 K), the simplified Eq. (10) underestimates the evaporation mass flux. The impact of the two equations on the thin-film calculation is shown in Fig. 7. Two different superheat levels are considered, 5 K and 20 K. It is seen that for superheats of up to 5 K, predictions from the two equations still agree well with each other. For very high values of superheat, such as those which may occur at the bottom of a bubble during nucleate boiling, Eq. (10) underestimates the heat transfer and results in a flatter thickness profile.

Fig. 7 also investigates the influence of approximations made in the evaluation of the coefficients a and b in Eq. (10). The interfacial temperature T_{lv} in the coefficients a and b has been commonly replaced by T_w [28] for convenience in the literature. This is appropriate when the wall superheat is small, so that $T_{lv} \approx T_w$. For high superheat, however, it is more appropriate to use $T_{lv} \approx T_v$, as seen in the figure.

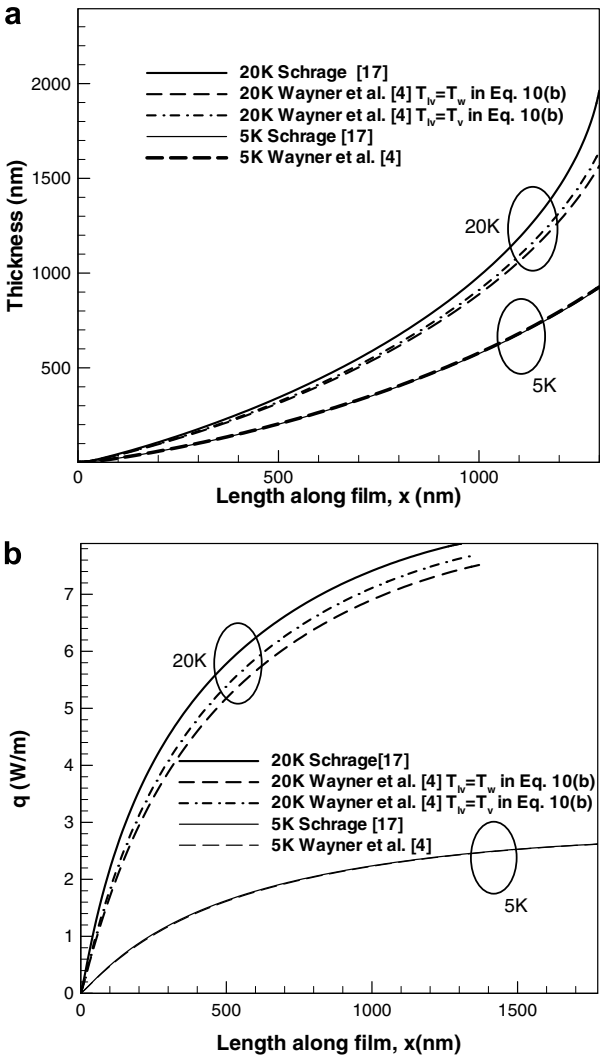

Fig. 7. Comparison between thin film predictions from Eq. (7) [17] and Eq. (10) [4] for different values of superheat ($R^* = 2500$ nm): (a) thickness profile, and (b) cumulative q.

3.4. Suppression of interface mass transport due to capillary pressure

While the suppression effect of disjoining pressure on thin-film evaporation has been widely discussed [4–6,9,10], a similar discussion of the effect of capillary pressure has seldom been reported. The interfacial evaporation heat transfer coefficient h_{lv} is plotted in Fig. 8 for wall superheats of 0.1 K and 1 K. It is clear that h_{lv} is suppressed in the beginning due to the disjoining pressure as has been extensively discussed in the literature [4–10]. After a peak at $x \approx 400$ nm, h_{lv} is seen to decrease again, this time because of the suppression due to capillary pressure. If the suppression due to capillary pressure were ignored, h_{lv} would follow the dashed line in the figure and approach a higher constant value of 1.04×10^6 W/m^2 K, which is consistent with published values of h_{lv} for situations that do not encounter suppression effects due to capillary pressure [17].

The drop in h_{lv} is more significant for lower T_{lv}. If the wall superheat is increased from 0.1 K to 1 K, the interface temperature is greater, and the restraining effect becomes less significant, as shown in the figure. This trend can also be deduced from Eq. (10)by using definition of h_{lv}:

$$h_{lv} = h_{fg}\left[a - b(p_d + p_c)\frac{1}{(T_{lv} - T_v)}\right] \tag{12}$$

where h_{fg} is the latent heat of evaporation. It is seen that a smaller $(T_{lv} - T_v)$ amplifies the second term in the brackets, which represents the suppression of h_{lv}. When $(T_{lv} - T_v)$ is small enough, based on this equation, h_{lv} can even take a negative value.

It may be noted from the figure that even though the capillary pressure approaches a constant value beyond $x \approx 400$ nm, h_{lv} continues to decrease because of the continuous drop in interface temperature T_{lv}. As T_{lv} decreases with increasing film thickness, the restraining effect of P_c increases.

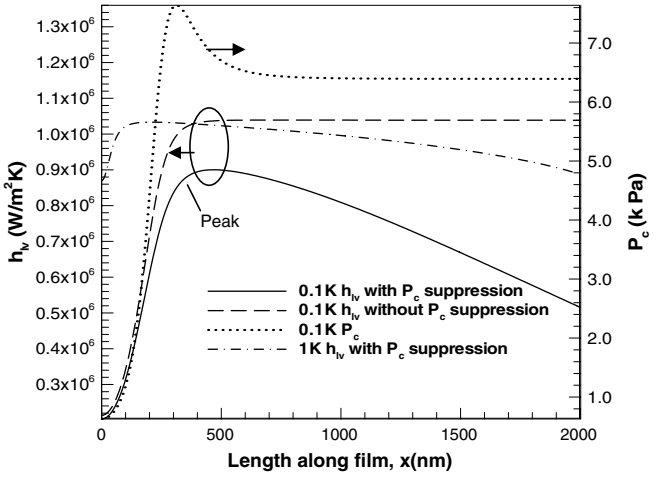

Fig. 8. Interface heat transfer coefficient along the meniscus. Heat transfer is suppressed by the disjoining pressure to the left of the peak and by capillary pressure to the right. Lower superheat results in stronger suppression ($R^* = 2500$ nm).

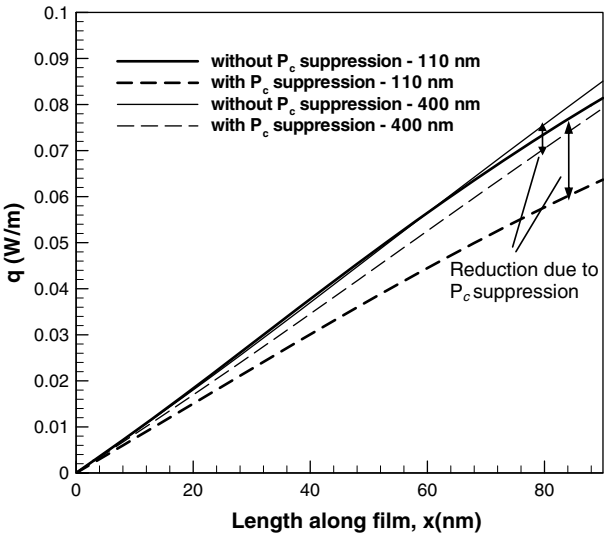

Fig. 9. Capillary suppression of cumulative heat transfer for different channel sizes ($R^* = 110$ and 400 nm); the smaller channel size results in greater suppression.

The restraining effect of capillary pressure is also seen to be more significant for smaller channels as shown in Fig. 9, since the intrinsic meniscus has greater curvature and capillary pressure is stronger in the smaller channels.

Finally, a higher dispersion constant A is known to result in a longer thin-film region and to promote heat transfer [4–10]. A higher capillary pressure (due to a higher value of surface tension) also flattens the film profile. The flattened profile shown in Fig. 10 has smaller thickness and the heat transfer is expected to be enhanced. However, the heat transfer is not always enhanced as shown in Fig. 10 because higher capillarity also causes greater suppression of evaporation. In [9], the effect of fluid polarity was found to elongate the thin-film region and cause

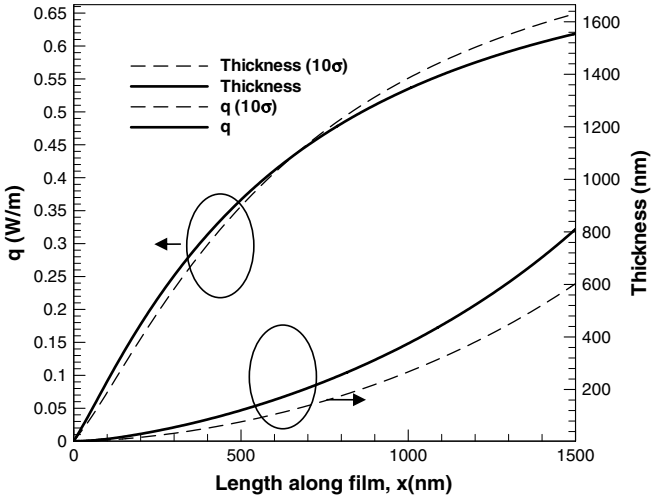

Fig. 10. Influence of increasing surface tension on cumulative heat transfer and film thickness ($R^* = 2500$ nm).

Table 3
Micro-region for (a) different channel sizes (superheat 1 K), and (b) different superheats ($R^* = 61$ μm)

(*a*)			
R^* (nm)	2500	6.1×10^4	2.1×10^5
Micro-region length (nm)	1653	3945	4275
q_m (W/m)	0.64	1.14	1.2
Percentage contribution to net heat transfer rate	97%	60%	50%

(*b*)		
Superheat (K)	1	5
Micro-region length (nm)	3945	2593
q_m (W/m)	1.14	3.70
Percentage contribution to net heat transfer rate	60%	56%

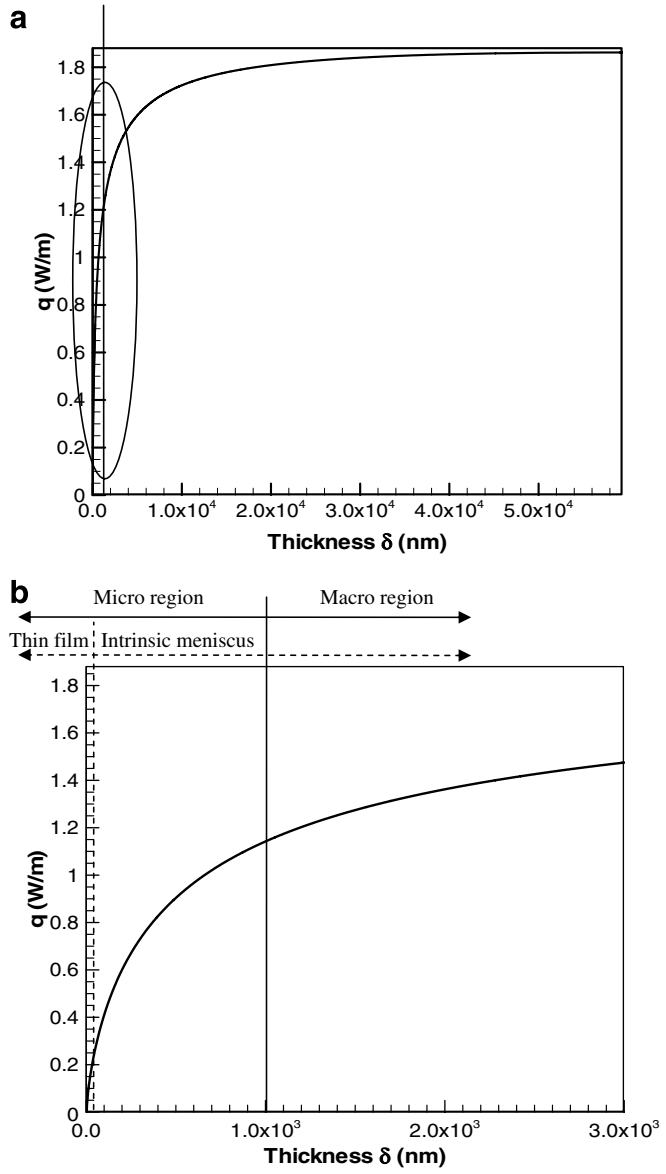

Fig. 11. Cumulative heat transfer q increase with thickness: (a) overall variation and (b) detail near origin. The solid line divides the micro and macro regions, while the dashed line divides the thin-film region and the intrinsic meniscus (superheat of 1 K, $R^* = 61$ μm).

stronger suppression, similar to the effects of capillary pressure discussed here.

4. Micro-region heat transfer

In this work, the micro-region of a meniscus is defined as the region in which the film thickness is less than 1 μm. The region with film thickness greater than 1 μm is referred to as the macro region. Table 3(a) and (b) shows the length and heat transfer of the micro-region for different channel sizes and superheats. The length of the micro-region is seen to be more than ten times that of the thin-film region, which is typically about 100 nm in length (Table 2(a)).

It was previously seen from Table 2(a) that the thin-film heat transfer q_t is not very significant for large microchannels. For example, for $R^* = 61$ μm, q_t is only 8% of the overall heat transfer. However, Fig. 11 and Table 3(b) show that the micro-region is responsible for 60% of the overall heat transfer in the same channel. The results under different superheats and channel sizes are listed in Table 3(a) and (b). In Stephan and Busse's study of an ammonia meniscus in a groove of 1 mm height and 1 mm width [12], 45% of the overall heat transfer was found to be dissipated from the micro-region, consistent with the calculations in the present study. It is concluded that the micro-region is, in general, much more important to the overall heat transfer than is the thin film for the range of parameters considered here.

It is also found that the temperature drop along the interface mainly occurs within micro-region rather than in the macro region. As shown in Fig. 12, T_{lv} drops sharply in the micro-region (of 3.94 μm length) from 344 K to 343.1 K, accounting for 90% of the total drop. In the macro region, the interfacial temperature is close to the

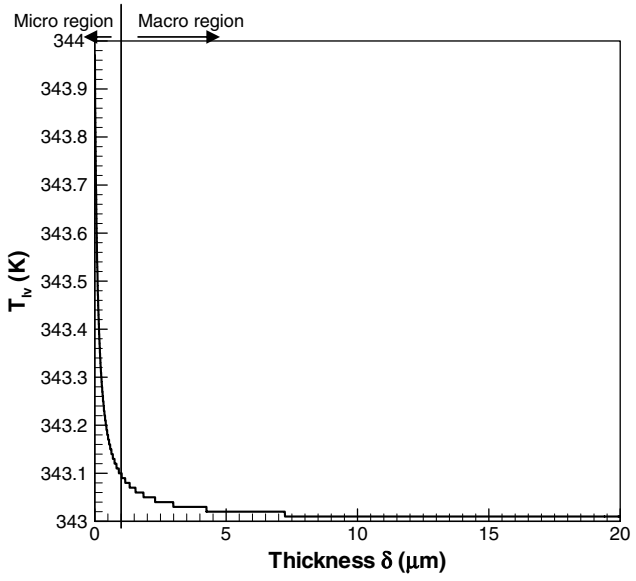

Fig. 12. Decrease in interfacial temperature along the liquid film; 90% of the temperature drop occurs within the micro-region.

saturation temperature, and can drive relatively little evaporation. In the thin-film region (of 160 nm length), the drop is from 344 K to 343.8 K, which is about 20% of the total drop.

5. Conclusions

The thin-film region of an evaporating meniscus is investigated through an augmented Young–Laplace model. The boundary conditions for the film profile are discussed in detail. The primary conclusions of the study are summarized below.

1. The thin-film region of the extended meniscus is delineated. The influence of channel radius on heat transfer rate is found to be most pronounced in the intrinsic meniscus and not in the thin-film region. The contribution of the thin-film region to the overall heat transfer is inversely proportional to the channel size and wall superheat. In a microchannel with a superheat of greater than 1 K, the thin film is shown to contribute less than 20% of the total heat transfer from the liquid film.
2. The micro-region is seen to be the major contributor to the overall heat transfer from the extended meniscus. It consists of the thin-film region and a part of the intrinsic meniscus. More than 50% of the overall heat transfer and 90% of the interfacial temperature drop occur in the micro-region for the conditions considered here.
3. The original mass transport expression without approximations is employed to study a wide superheat range and is compared to the simplified expression that has been widely used in the literature [4]. The simplified expression is found to significantly underestimate the interfacial evaporation heat transfer coefficient for superheats above 5 K, and induces significant deviations in the computed thin-film profile for superheats above 20 K.
4. Capillary pressure plays an important role in determining the film profile throughout the extended meniscus. Its effect on suppressing evaporation is significant for small channels and low superheats.

Acknowledgement

The authors acknowledge financial support for this work from members of the Cooling Technologies Research Center (www.ecn.purdue.edu/CTRC), a National Science Foundation Industry/University Cooperative Research Center at Purdue University.

References

[1] B.V. Deryagin, S.V. Nerpin, N.V. Churayev, Effect of film heat transfer upon evaporation of liquids from capillaries, Bull. R. I. L. E. M. 29 (1965) 93–98.
[2] B.V. Deryagin, Modern state of the investigation of long-range surface forces, Langmuir 3 (5) (1987) 601–606.
[3] M. Potash Jr., P.C. Wayner Jr., Evaporation from a two-dimensional extended meniscus, Int. J. Heat Mass Transfer 15 (1972) 1851–1863.
[4] P.C. Wayner Jr., Y.K. Kao, L.V. LaCroix, The interline heat transfer coefficient of an evaporating wetting film, Int. J. Heat Mass Transfer 19 (1976) 487–492.
[5] J.A. Schonberg, P.C. Wayner Jr., Analytical solution for the integral contact line evaporation heat sink, in: Proceedings of the AIAA/ASME 5th Joint Thermophysics and Heat Transfer Conference, Seattle, AIAA-1990-1787, 1990.
[6] K.P. Hallinan, H.C. Chebaro, S.J. Kim, W.S. Chang, Evaporation from an extended meniscus for nonisothermal interfacial conditions, J. Thermophys. Heat Transfer 8 (1994) 709–716.
[7] S. DasGupta, J.A. Schonberg, P.C. Wayner Jr., Investigation of an evaporating extended meniscus based on the augmented Young–Laplace Equation, J. Heat Mass Transfer 115 (1993) 201–208.
[8] K. Park, K. Noh, K. Lee, Transport phenomena in the thin-film region of a micro-channel, Int. J. Heat Mass Transfer 46 (2003) 2381–2388.
[9] S.K. Wee, Microscale Observables for Heat and Mass Transport, Ph.D. Thesis, Texas A&M University, 2004.
[10] S. Wee, K.D. Kihm, D.M. Pratt, J.S. Allen, Microscale heat and mass transport of evaporating thin film of binary mixture, J. Thermophys. Heat Transfer 20 (2006) 320–327.
[11] J.B. Freund, The atomic detail of an evaporating meniscus, Phys. Fluids 17 (2005) 022104.
[12] P.C. Stephan, C.A. Busse, Analysis of the heat transfer coefficient of grooved heat pipe evaporator walls, Int. J. Heat Mass Transfer 35 (1992) 383–391.
[13] X. Xu, V.P. Carey, Film evaporation from a micro-grooved surface – an approximate heat transfer model and its comparison with experimental data, J. Thermophys. Heat Transfer 4 (1990) 512–520.
[14] H.B. Ma, G.P. Peterson, Temperature variation and heat transfer in triangular grooves with an evaporating film, J. Thermophys. Heat Transfer 11 (1997) 90–97.
[15] S.J.S. Morris, The evaporating meniscus in a channel, J. Fluid Mech. 494 (2003) 297–317.
[16] C. Chakraborty, S.K. Som, Heat transfer in an evaporating thin liquid film moving slowly along the walls of an inclined microchannel, Int. J. Heat Mass Transfer 48 (2005) 2801–2805.
[17] R.W. Schrage, A Theoretical Study of Interface Mass Transfer, Columbia University Press, New York, 1953.
[18] B.V. Derjaguin, Z.M. Zorin, Optical study of the adsorption and surface condensation of vapours in the vicinity of saturation on smooth surface, in: Proceedings of the Second International Conference of Surface Activity, vol. 2, 1957, pp.145–152.
[19] V.P. Carey, Liquid–vapor Phase-change Phenomena, Hemisphere Publishing House, New York, 1992.
[20] D.J.E. Harvie, D.F. Fletcher, A simple kinetic theory treatment of volatile liquid–gas interfaces, J. Heat Transfer 123 (2001) 487–491.
[21] A. Faghri, Heat Pipe Science and Technology, Taylor & Francis, Washington, DC, 1995.
[22] B. Paul, Complication of evaporation coefficients, Am. Rocket Soc. J. 32 (1962) 1321–1328.
[23] J.A. Schonberg, S. DasGupta, P.C. Wayner Jr., An augmented Young–Laplace model of an evaporation meniscus in a microchannel with high heat flux, Exp. Therm. Fluid Sci. 10 (1995) 163–170.
[24] J.G. Truong, P.C. Wayner Jr., Effect of capillary and van der Waals dispersion force on the equilibrium profile of a wetting fluid: theory and experiment, J. Chem. Phys. 87 (1987) 4180–4188.
[25] J.R. Dormand, P.J. Prince, A family of embedded Runge–Kutta formulae, J. Comput. Appl. Math. 6 (1980) 19–26.
[26] L.W. Swanson, G.C. Herdt, Model of the evaporating meniscus in a capillary tube, J. Heat Transfer 114 (1992) 434–441.
[27] D. Welter, The Effect of Evaporation on the Dynamic Capillary Pressure in Heat Pipes, Master's Thesis, University of Dayton, Ohio, 1991.
[28] R. Marek, J. Straub, Analysis of the evaporation coefficient and the condensation coefficient of water, Int. J. Heat Mass Transfer 44 (2001) 39–53.